united nations
educational, scientific
and cultural
organization

international atomic
energy agency

the
abdus salam
international centre for theoretical physics

H4.SMR/1519-12

"Seventh Workshop on Non-Linear Dynamics and Earthquake Prediction"

29 September - 11 October 2003

Fundamentals of Damage Mechanics

D. L. Turcotte

Department of Geology
University of California Davis
CA 95616-8605
USA

ELSEVIER

Available online at www.sciencedirect.com
SCIENCE DIRECT®

Theoretical and Applied Fracture Mechanics 39 (2003) 245–258

theoretical and applied fracture mechanics

www.elsevier.com/locate/tafmec

Damage and self-similarity in fracture

R. Shcherbakov *, D.L. Turcotte

Department of Earth and Atmospheric Sciences, Snee Hall, Cornell University, Ithaca, NY 14853, USA

Abstract

Consider applications of damage mechanics to material failure. The damage variable introduced in damage mechanics quantifies the deviation of a brittle solid from linear elasticity. An analogy between the metastable behavior of a stressed brittle solid and the metastable behavior of a superheated liquid is established. The nucleation of microcracks is analogous to the nucleation of bubbles in the superheated liquid. In this paper we have applied damage mechanics to four problems. The first is the instantaneous application of a constant stress to a brittle solid. The results are verified by applying them to studies of the rupture of chipboard and fiberglass panels. We then obtain a solution for the evolution of damage after the instantaneous application of a constant strain. It is shown that the subsequent stress relaxation can reproduce the modified Omori's law for the temporal decay of aftershocks following an earthquake. Obtained also are the solutions for application of constant rates of stress and strain. A fundamental question is the cause of the time delay associated with damage and microcracks. It is argued that the microcracks themselves cause random fluctuations similar to the thermal fluctuations associated with phase changes.

Keywords: Damage mechanics; Fracture; Critical point; Power-law scaling

1. Introduction

The inelastic behavior of solid materials is characterized by a wide range of processes; examples include decohesion between inclusions, accumulation of dislocations leading to the nucleation of microcracks, debonding of fibers and matrix in composite materials, etc. This irreversible behavior is often referred to as *damage* [1–3]. A damage variable α can be introduced that is the measure of deviations from linear elasticity. The evolution of damage is specified by a rate equation. Thermally activated creep processes (diffusion and dislocation creep), the plastic deformation of ductile materials beyond a threshold and the rupture of brittle materials are examples of damage. In this paper we will concentrate our attention on the irreversible deformation of solids associated with their brittle failure.

The brittle failure of a solid is certainly a complex phenomenon that has received a great deal of attention from engineers, geophysicists, and physicists. A limiting example of brittle failure is the propagation of a single fracture through a homogeneous solid. However, this is an idealized case that requires a preexisting crack or notch to

* Corresponding author.
E-mail addresses: rs120@cornell.edu (R. Shcherbakov), turcotte@geology.ucdavis.edu (D.L. Turcotte).

0167-8442/03/$ - see front matter
doi:10.1016/S0167-8442(03)00005-3

concentrate the applied stress. Even the propagation of a single fracture is poorly understood because of the singularities at the crack tip [4]. In most cases, the fracture of a homogeneous brittle solid involves the generation of microcracks. Initially these microcracks are randomly distributed, as their density increases they coalesce and localize until a through-going rupture results. This process depends upon the heterogeneity of the solid.

Many experiments on the fracture of brittle solids have been carried out. In terms of rock failure, the early experiments [5] were pioneering. Acoustic emissions (AE) associated with microcracks were monitored and power-law frequency-magnitude statistics were observed for the AE. When a load was applied very rapidly, the time-to-failure was found to depend on the load. Many other studies of this type have been carried out. Obtained in [6] is the statistical distribution of the life times with constant stress loading for carbon fiber–epoxy microcomposites. The work in [7] studied the rupture of spherical tanks of kevlar wrapped around thin metallic liners and found a power-law increase of AE prior to rupture. The failure of chipboard and fiberglass panels were considered in [8,9]. They obtained power-law increases in AE prior to rupture and a systematic dependence of failure times on stress level.

Statistical physicists have related brittle rupture to liquid–vapor phase changes in a variety of ways. A first-order phase transition was related [10] to brittle fracture. Similar arguments have been given by Zapperi et al. [11] and Kun and Herrmann [12]. On the other hand it was argued [13,14] that brittle rupture is analogous to a critical point phenomena, not to a first-order phase change. They associated observed power-law scaling in brittle failure experiments with a critical point (a second-order phase change). A number of authors have considered brittle rupture in analogy to spinodal nucleation [15–19]. This analogy is studied in more detail in the next section.

2. Damage mechanics

In order to provide a basis for discussing material failure as a phase change process, we first discuss the phase diagram for the coexistence of the liquid and vapor phases of a pure substance. A schematic pressure-volume projection of a phase diagram is illustrated in Fig. 1(a) [20]. The ratio of

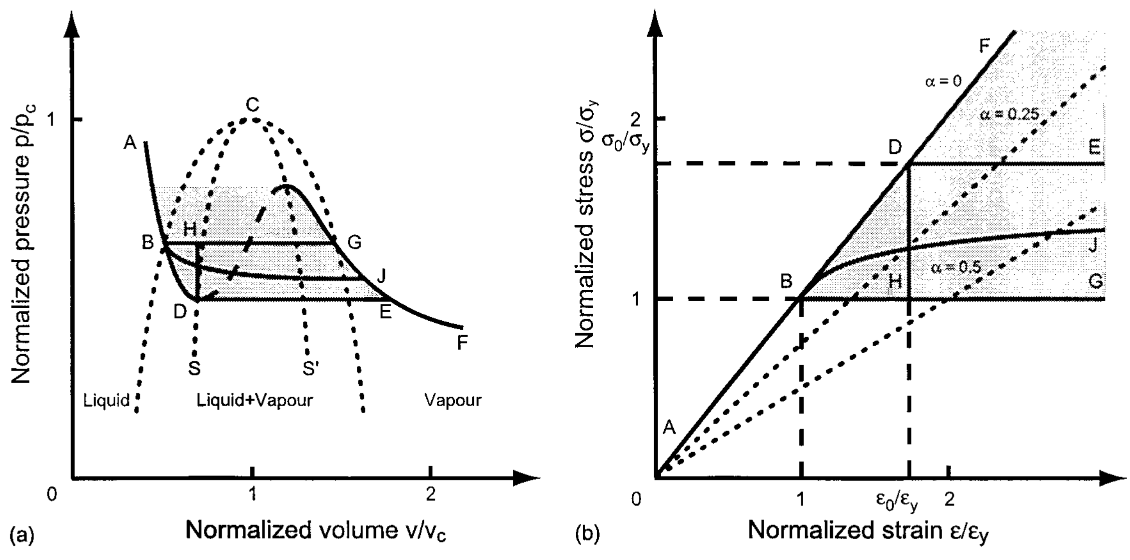

Fig. 1. (a) Schematic pressure–volume projection of the phase diagram of a pure substance [20]. The shaded region is metastable. (b) Idealized stress–strain diagram for a brittle solid. The shaded region is in a damaged state.

the pressure p to the pressure at the critical point C, p_c, is given as a function of the ratio of the specific volume v to the specific volume at the critical point v_c. We consider a liquid initially at point A in the figure. The pressure is decreased isothermally until the phase change boundary is reached at point B. In thermodynamic equilibrium the liquid will boil at constant pressure and temperature until it is entirely a vapor at point G. Further reduction of pressure will result in the isothermal expansion of the vapor along the path GF. However, it is possible to create a metastable, superheated liquid at point B. If bubbles of vapor do not form, either by homogeneous or heterogeneous nucleation, the liquid can be superheated along the path BD. The point D is the intersection of the liquid P–V curve with the spinodal curve S. It is not possible to superheat the liquid beyond this point. If the liquid is superheated to the vicinity of point D, explosive nucleation and boiling will take place. If the pressure and temperature are maintained constant during this highly nonequilibrium explosion, the substance will follow the path DE to the vapor equilibrium curve GF. If the explosion occurs at constant volume and temperature, the pressure will increase as the substance follows the path DH to the equilibrium boiling line BG. With a combination of bubble nucleation and superheating other paths through the shaded metastable region are possible. A typical path BJ is illustrated.

Next apply the concept of phase change to the brittle fracture of a solid. For simplicity we will discuss the failure of a sample of area a under compression by a force F. The state of the sample is specified by the stress $\sigma = F/a$ and its strain $\epsilon = (L_0 - L)/L_0$ (L length, L_0 initial length). The dependence of the stress on strain is illustrated schematically in Fig. 1(b). At low stresses we assume that Hooke's law is applicable so that

$$\sigma = E_0\epsilon, \tag{1}$$

where E_0 is Young's modulus, a constant.

We hypothesize that a pristine brittle solid will obey linear elasticity for stresses in the range $0 \leqslant \sigma \leqslant \sigma_y$, where σ_y is a yield stress. From Eq. (1) the corresponding yield strain ϵ_y is given by

$$\epsilon_y = \frac{\sigma_y}{E_0}. \tag{2}$$

If stress is applied infinitely slowly (to maintain a thermodynamic equilibrium), we further hypothesize that the solid will fail at the yield stress σ_y. The failure path ABG in Fig. 1(b) corresponds to the equilibrium failure path ABG in Fig. 1(a). This is equivalent to perfectly plastic behavior.

If an elastic solid is loaded very rapidly with a constant stress $\sigma_0 > \sigma_y$ applied instantaneously, the solid will satisfy Eq. (1) and will follow the path ABD as shown in Fig. 1(b), subsequently, damage will occur at a constant stress along the path DE until the solid fails. This behavior is analogous to the constant pressure boiling that occurs along the path DE in Fig. 1(a).

Alternatively the elastic solid could be strained very rapidly with a constant strain $\epsilon_0 > \epsilon_y$ applied instantaneously, again the solid will satisfy Eq. (1) and will follow the path ABD as shown in Fig. 1(b). In this case damage will occur along the constant strain path DH until the stress is reduced to the yield stress σ_y. This behavior is analogous to the constant volume boiling that occurs along the path DH in Fig. 1(a).

When the stress on a brittle solid is increased at a constant finite value we hypothesize that linear elasticity (1) is applicable in the range $0 \leqslant \sigma \leqslant \sigma_y$. At stresses greater than the yield stress, $\sigma > \sigma_y$, damage occurs in the form of microcracks. This damage results in accelerated strain and a deviation from linear elasticity. A typical failure path ABJ is illustrated in Fig. 1(b). In order to quantify the deviation from linear elasticity, the damage variable α is introduced in the strain–stress relation

$$\sigma = E_0(1 - \alpha)\epsilon. \tag{3}$$

When $\alpha = 0$, Eq. (3) reduces to Eq. (1) and linear elasticity is applicable; as $\alpha \to 1$ ($\epsilon \to \infty$) failure occurs. Positions in the stress–strain plot, Fig. 1(b), corresponding to $\alpha = 0.0$, 0.25, and 0.5 are shown by dashed lines.

It must be emphasized that the analogy between boiling and fracture illustrated in Fig. 1 is not complete. Boiling is a reversible process, fracture is not. However, we believe the analogy is illustrative.

Based upon thermodynamic considerations [1, 3,21], the time evolution of the damage variable is related to the time dependent stress $\sigma(t)$ and strain $\epsilon(t)$ by

$$\frac{\mathrm{d}\alpha(t)}{\mathrm{d}t} = A(\sigma(t))\left[\frac{\epsilon(t)}{\epsilon_y}\right]^2. \tag{4}$$

It should be noted that there are alternative formulations of both Eqs. (3) and (4) and that $A(\sigma)$ can take many forms [3]. This analysis assumes that Eqs. (3) and (4) are applicable and will further require that

$$A(\sigma(t)) = 0 \quad \text{if } 0 \leqslant \sigma \leqslant \sigma_y \tag{5}$$

$$A(\sigma(t)) = \frac{1}{t_d}\left[\frac{\sigma(t)}{\sigma_y} - 1\right]^{\rho} \quad \text{if } \sigma > \sigma_y, \tag{6}$$

where t_d is a characteristic time scale for damage and ρ is a power to be determined from experiments. This formulation will be confirmed by a direct comparison with experiments.

The monotonic increase in the damage variable α given by Eqs. (4)–(6) represents the weakening of the brittle solid due to the nucleation and coalescence of microcracks. This nucleation and coalescence of microcracks is analogous to the nucleation and coalescence of bubbles in a superheated liquid as discussed above. A brittle solid in the shaded region in the stress–strain diagram given in Fig. 1(b) is metastable in the same sense that the nonequilibrium boiling in the shaded region in Fig. 1(a) is metastable.

Solutions to one-dimensional damage problems require the simultaneous solution of Eqs. (3)–(6). In general it is required that either the stress or the strain on the sample be specified. Consider four examples:

(i) Assume that a constant stress σ_0 is applied instantaneously at $t = 0$. If $\sigma_0 \leqslant \sigma_y$ no damage occurs and the strain is given by Eq. (1). If $\sigma_0 > \sigma_y$ the material is strained elastically into the metastable region along the path ABD in Fig. 1(b). The stress is then maintained at σ_0 until the sample fails. Our solution will give the time to failure t_f as a function of the applied stress σ_0 and the time dependence of the damage variable $\alpha(t)$ and the strain $\epsilon(t)$. The sample fails along the path DE in Fig. 1(b). This solution with experiments.

(ii) Assume that a constant strain ϵ_0 is applied instantaneously at $t = 0$. If $\epsilon_0 \leqslant \epsilon_y$ no damage occurs and the stress is given by Eq. (1). If $\epsilon_0 > \epsilon_y$ the material is strained elastically into the metastable region along the path ABD in Fig. 1(b). The strain is maintained at ϵ_0 as damage occurs. Because of the damage, the stress on the sample relaxes from the initial value σ_0 to the yield stress σ_y. This stress relaxation takes place along path DH illustrated in Fig. 1(b). The solution will give the time dependence of the damage variable $\alpha(t)$ and stress $\sigma(t)$ during the relaxation. The application of this solution to earthquake aftershocks will be discussed.

(iii) Assume that the applied stress σ is increased linearly with time t. Initially with $\sigma \leqslant \sigma_y$ the strain is given by Eq. (1) and the path AB is followed in Fig. 1(b). But when the stress $\sigma > \sigma_y$, damage occurs until the sample fails. A typical failure path is given by BJ in Fig. 1(b). It will be shown that the path through the metastable region depends on the rate at which the stress is increased.

(iv) Assume that the applied strain ϵ is increased linearly with time t. Initially with $\epsilon \leqslant \epsilon_y$ the stress is given by Eq. (1) and the path AB is followed in Fig. 1(b). But when the strain $\epsilon > \epsilon_y$, damage occurs. Stress relaxation occurs as in example (ii) discussed above.

3. Constant applied stress

As a first example, consider a rod to which a constant axial tensional stress has been applied. A stress $\sigma_0 > \sigma_y$ is applied instantaneously at $t = 0$ and held constant until the sample fails. The applicable equation for the rate of increase of damage with time is obtained from Eqs. (2), (4), and (6) with the result

$$\frac{\mathrm{d}\alpha}{\mathrm{d}t} = \frac{1}{t_d}\left(\frac{\sigma_0}{\sigma_y} - 1\right)^{\rho}\left[\frac{E_0\epsilon(t)}{\sigma_y}\right]^2. \tag{7}$$

From Eq. (3) the strain ϵ is related to the damage variable α and the constant applied stress σ_0 by

$$\epsilon(t) = \frac{\sigma_0}{E_0[1-\alpha(t)]}. \tag{8}$$

Substitution of Eqs. (8) into (7) gives the damage rate

$$\frac{d\alpha}{dt} = \frac{1}{t_d}\left(\frac{\sigma_0}{\sigma_y}\right)^2\left(\frac{\sigma_0}{\sigma_y}-1\right)^\rho \frac{1}{[1-\alpha(t)]^2}. \tag{9}$$

Integrating with the initial condition $\alpha(0) = 0$, there results

$$\alpha(t) = 1 - \left[1 - \frac{3t}{t_d}\left(\frac{\sigma_0}{\sigma_y}\right)^2\left(\frac{\sigma_0}{\sigma_y}-1\right)^\rho\right]^{1/3}, \tag{10}$$

which describes the damage evolution in the material with constant applied stress. Using Eq. (10), Eq. (8) can be rewritten as

$$\epsilon(t) = \frac{\sigma_0}{E_0\left[1 - \frac{3t}{t_d}\left(\frac{\sigma_0}{\sigma_y}\right)^2\left(\frac{\sigma_0}{\sigma_y}-1\right)^\rho\right]^{1/3}}. \tag{11}$$

Failure occurs at the time t_f when $\alpha \to 1$ ($\epsilon \to \infty$); thus we obtain the time of failure t_f in terms of the characteristic damage time t_d, yield stress σ_y and applied stress σ_0

$$t_f = \frac{t_d}{3}\left(\frac{\sigma_y}{\sigma_0}\right)^2\left(\frac{\sigma_0}{\sigma_y}-1\right)^{-\rho}. \tag{12}$$

The time to failure approaches infinity as a power law as $\sigma_0 \to \sigma_y$. Substituting Eq. (12) into Eq. (10), the expression for the damage evolution is found:

$$\alpha(t) = 1 - \left(1 - \frac{t}{t_f}\right)^{1/3} \tag{13}$$

and for the corresponding time dependence of the strain

$$\epsilon(t) = \frac{\sigma_0}{E_0\left(1 - \frac{t}{t_f}\right)^{1/3}}. \tag{14}$$

The approach to failure is in the form of a power law.

Now compare the results derived above with experiments. Guarino et al. studied in [9] the failure of circular panels (222 mm diameter, 3–5 mm thickness) of chipboard and fiberglass. A differential pressure was applied rapidly across a panel and was held constant until the panel failed. Acoustic emission (AE) events associated with microcracks were carefully monitored, located and quantified. For these relatively thin panels, bending stresses were negligible and the panels failed under tension (a mode I fracture). Initially, the microcracks appeared to be randomly distributed across the panel; as the number of microcracks increased they tended to localize and coalesce in the region where the final rupture occurred. These authors measured the cumulative energy in the AE events e_{AE} as a function of time t. The total AE energy at the time of rupture is e_{tot}. The observed dependence of e_{AE}/e_{tot} on $(1 - t/t_f)$ for these experiments is given in Fig. 2(a). After an initial transient period ($0 < t/t_f < 0.4$), good power-law scaling was observed. In this scaling region it was found that $e_{AE} \propto (1 - t/t_f)^{-0.27}$. This is equivalent to having $de_{AE}/dt \propto (1 - t/t_f)^{-1.27}$.

Next, relate the rate of increase of the damage variable $d\alpha/dt$ to the rate of AE. The approach is illustrated in Fig. 3(a). The elastic energy density e_{ab} in the rod after the instantaneous stress σ_0 has been applied is

$$e_{ab} = \frac{\sigma_0^2}{2E_0}. \tag{15}$$

The work done on the rod at constant stress σ_0 along the path bc is given by

$$e_{bc} = \sigma_0(\epsilon_c - \epsilon_b) \tag{16}$$

and the strain ϵ_c is given by

$$\epsilon_c = \frac{\sigma_0}{E_0(1-\alpha)}. \tag{17}$$

Substitution of Eqs. (1) and (17) into (16) gives

$$e_{bc} = \frac{\sigma_0^2\alpha}{E_0(1-\alpha)}. \tag{18}$$

It is hypothesized that if the applied stress is instantaneously removed at point c then the rod will follow the path ca. The elastic energy recovered along this path is

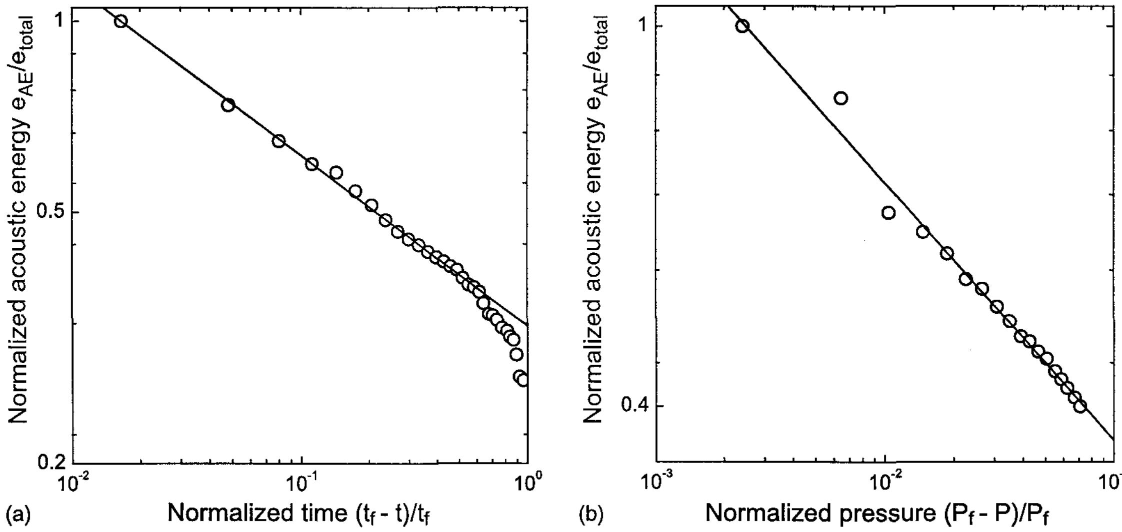

Fig. 2. (a) Normalized cumulative acoustic energy emissions $e_{\mathrm{AE}}(t)/e_{\mathrm{tot}}$ as a function of $(1 - t/t_{\mathrm{f}})$ in the case of a constant applied pressure difference [9]. (b) Normalized cumulative acoustic energy emissions $e_{\mathrm{AE}}(t)/e_{\mathrm{tot}}$ as a function of $(P_{\mathrm{f}} - P)/P_{\mathrm{f}}$. The applied pressure difference P across the panel increased linearly with time in accordance with (37) [8].

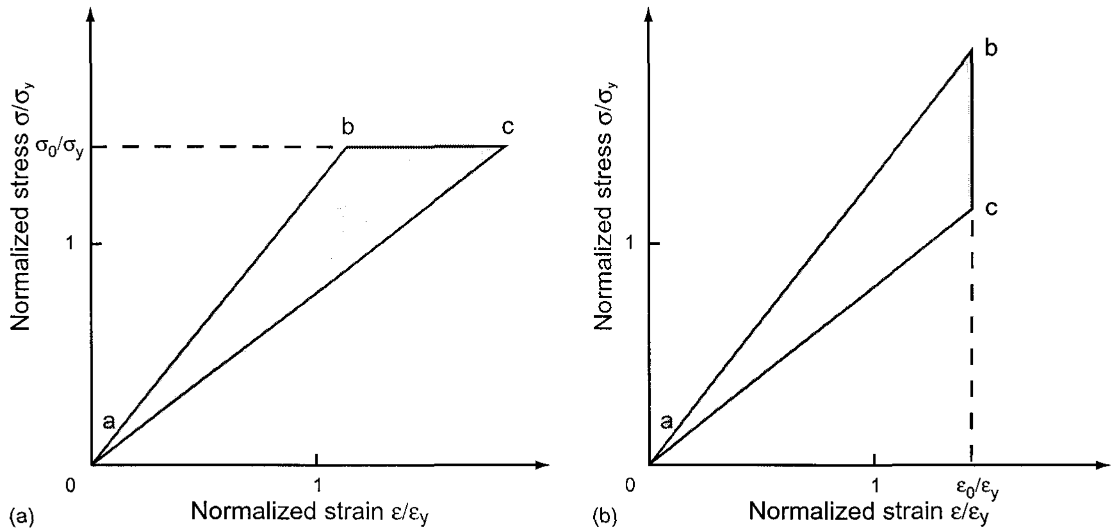

Fig. 3. Illustration of the determination of energy release e_{AE} (the areas in the shaded regions) in AE. (a) Instantaneous application of a constant stress σ_0 along the path ab. (b) Instantaneous application of a constant strain ϵ_0 along the path bc.

$$e_{\mathrm{ca}} = \frac{\sigma_0^2}{2E_0(1-\alpha)}. \tag{19}$$

In addition the difference between the energy added $e_{\mathrm{ab}} + e_{\mathrm{bc}}$ and the energy recovered e_{ca} has been lost in AE. This energy e_{AE} corresponds to the area of the triangle abc in Fig. 3(a) and is given by

$$e_{\mathrm{AE}} = e_{\mathrm{ab}} + e_{\mathrm{bc}} - e_{\mathrm{ca}} = \frac{\sigma_0^2}{2E_0}\frac{\alpha}{(1-\alpha)}. \tag{20}$$

Substitution of the damage variable from Eq. (13) gives

$$e_{AE} = \frac{\sigma_0^2}{2E_0}\left[\frac{1}{\left(1-\frac{t}{t_f}\right)^{1/3}} - 1\right]. \tag{21}$$

Thus the predicted rate of AE is

$$\frac{de_{AE}}{dt} = \frac{\sigma_0^2}{6E_0 t_f}\left(1-\frac{t}{t_f}\right)^{-4/3}. \tag{22}$$

Damage mechanics predicts the same power-law behavior observed in the experiments with the power −4/3 versus the power 1.27 for the experiments.

The time to failure t_f of the wood panel was determined [9] as a function of the constant applied differential pressure P. In their paper they correlated their results with the empirical relation $t_f \propto \exp[(P_0/P)^{-4}]$, where P_0 is a characteristic pressure. Instead we reinterpret their results and consider the correlation of the time to failure t_f and the pressure excess above a yield pressure (stress), $(P - P_y)$. Taking $P_y = 0.38$ (atm) this correlation is given in Fig. 4. A good fit is obtained taking $t_f \propto (P - P_y)^{-2.25}$. With $(P/P_y - 1) \ll 1$, this result is in agreement with Eq. (10) if $\rho = 2.25$. It is concluded that the threshold pressure P_y corresponds to a yield stress σ_y for the samples. Failure only occurs when the applied stress exceeds the yield stress for the sample considered. We also would like to mention that the value of $P_y = 0.38$ (atm) was chosen from the assumption that the time to failure t_f depends on the excess pressure $(P - P_y)$ as a power law which is not obvious for real samples. Precise measurements of the yield stress for wood panels studied in [9] are required to confirm the aforementioned hypothesis.

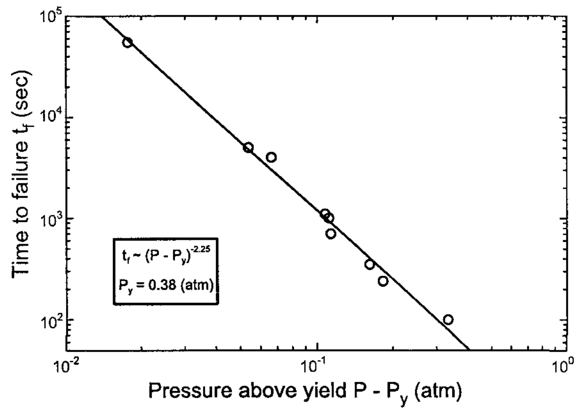

Fig. 4. Time to failure of a chipboard panel as a function of the excess pressure above a yield pressure, $P - P_y$; the pressure is applied instantaneously at $t = 0$ [9].

4. Constant applied strain

As a second example, consider a rod to which a constant axial compressive strain has been applied. A strain $\epsilon_0 > \epsilon_y$ is applied instantaneously at $t = 0$ and is held constant. The applicable equation for the rate of increase of damage is obtained from Eqs. (4) and (6) with the result

$$\frac{d\alpha}{dt} = \frac{1}{t_d}\left[\frac{\sigma(t)}{\sigma_y} - 1\right]^{\rho}\left(\frac{\epsilon_0}{\epsilon_y}\right)^2. \tag{23}$$

From (3) the stress σ is related to the damage variable α and the constant applied strain ϵ_0 by

$$\sigma(t) = E_0\epsilon_0[1 - \alpha(t)]. \tag{24}$$

Substitution of Eqs. (24) into (23) using (2) gives

$$\frac{d\alpha}{dt} = \frac{1}{t_d}\left(\frac{\epsilon_0}{\epsilon_y}\right)^2\left\{\frac{\epsilon_0}{\epsilon_y}[1 - \alpha(t)] - 1\right\}^{\rho}. \tag{25}$$

Integrating with the initial condition $\alpha(0) = 0$, it is found that

$$\alpha(t) = 1 - \frac{\epsilon_y}{\epsilon_0}\left\{1 + \left[\left(\frac{\epsilon_0}{\epsilon_y} - 1\right)^{-(\rho-1)} + (\rho - 1)\left(\frac{\epsilon_0}{\epsilon_y}\right)^3\left(\frac{t}{t_d}\right)\right]^{-1/\rho-1}\right\}. \tag{26}$$

The damage increases monotonically with time and as $t \to \infty$ the maximum damage is given by

$$\alpha(\infty) = 1 - \frac{\epsilon_y}{\epsilon_0}. \tag{27}$$

Using Eqs. (26) and (24) with (2) the stress relaxation in the material as a function of time t is obtained:

$$\frac{\sigma(t)}{\sigma_y} = 1 + \left[\left(\frac{\epsilon_0}{\epsilon_y} - 1\right)^{-(\rho-1)} + (\rho - 1)\left(\frac{\epsilon_0}{\epsilon_y}\right)^3\left(\frac{t}{t_d}\right)\right]^{-1/(\rho-1)}. \tag{28}$$

At $t = 0$, the relation

$$\sigma(0) = E_0\epsilon_0, \tag{29}$$

is recovered; it is the stress corresponding to the strain ϵ_0 from the linear elastic relation as expected. In the limit $t \to \infty$, there results

$$\sigma(\infty) = \sigma_y. \tag{30}$$

The stress relaxes to the yield stress σ_y below which no further damage can occur, again as expected. The nondimensional stress $\sigma(t)/\sigma_y$ from (28) is given as a function of nondimensional time t/t_d in Fig. 5(a) taking $\rho = 2$ and several values of the applied nondimensional strain ϵ_0/ϵ_y. High initial stresses relax quickly followed by a slow power-law relaxation. The nondimensional stress $\sigma(t)/\sigma_y$ from Eq. (28) is given as a function of nondimensional time t/t_f in Fig. 5(c) taking $\epsilon_0/\epsilon_y = 2$ and several values of the power-law exponent ρ. Increasing values of ρ greatly slow the stress relaxation.

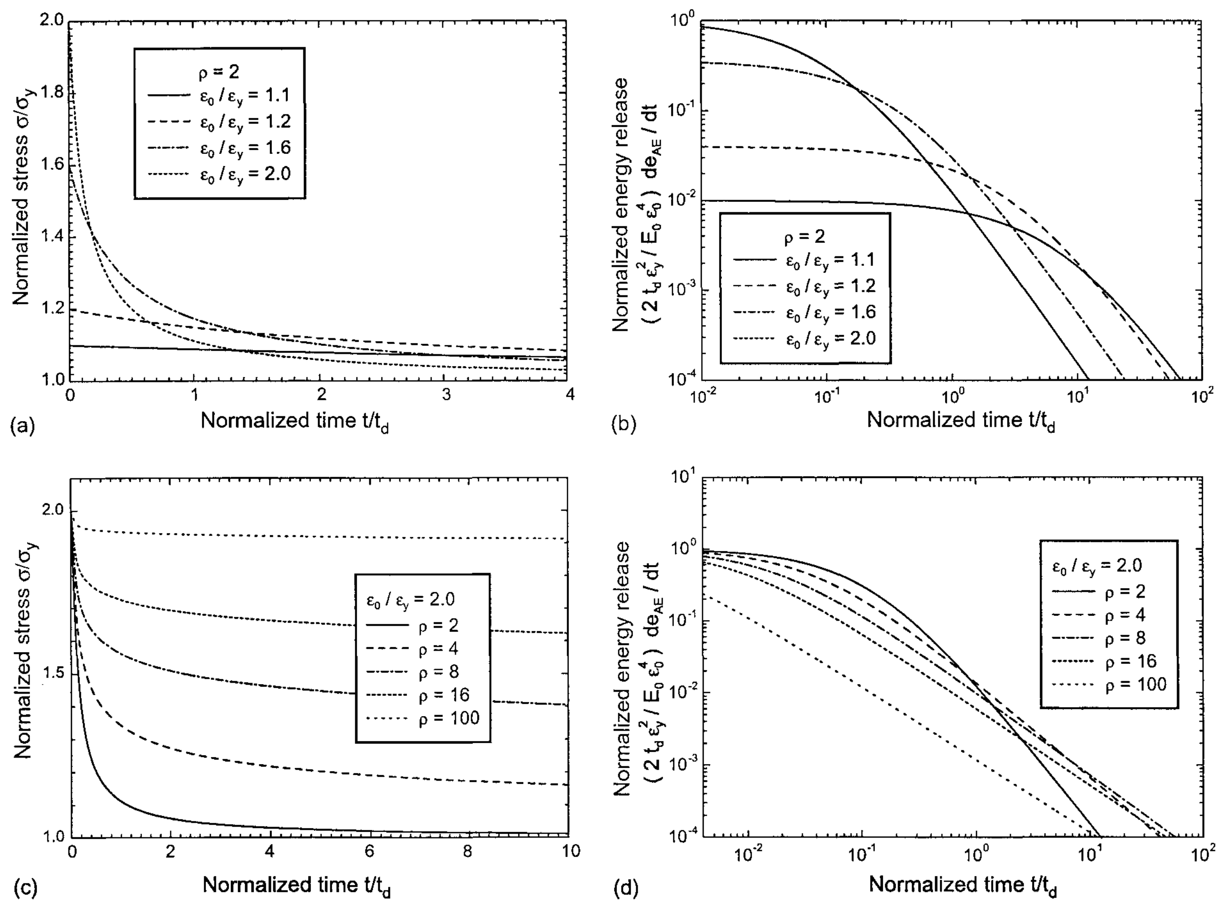

Fig. 5. (a) Stress relaxation after the instantaneous application of a constant strain ϵ_0 that exceeds the yield strain ϵ_y from (28). (b) The nondimensional rate of energy release $(2t_d\epsilon_y^2/E_0\epsilon_0^4)\mathrm{d}e/\mathrm{d}t$ after the instantaneous application of a constant strain ϵ_0 from (34). (c) Dependence of the nondimensional stress σ/σ_y on the nondimensional time t/t_f from (34). (d) The nondimensional rate of energy release $(2t_d\epsilon_y^2/E_0\epsilon_0^4)\mathrm{d}e/\mathrm{d}t$.

This stress relaxation process is applicable to the understanding of the aftershock sequence that follows an earthquake. During an earthquake some regions in the vicinity of the earthquake experience a rapid increase of stress (strain). This is in direct analogy to the rapid increase in strain considered. However, the stress σ is greater than the yield stress σ_y and microcracks (aftershocks) relax the stress to σ_y just as described above. The time delay of the aftershocks relative to the main shock is in direct analogy to the time delay of the damage. This delay is because it takes time to nucleate microcracks (aftershocks).

In order to quantify the rate of aftershock occurrence, the rate of energy release is determined for the relaxation process considered above. The present approach is illustrated in Fig. 3(b). The elastic energy density (per unit mass) e_{ab} in the rod after the instantaneous strain has been applied along the path ab is

$$e_{ab} = \frac{E_0\epsilon_0^2}{2} \tag{31}$$

Stress relaxation along path bc occurs at constant strain so that no work is done on the sample. Again it is hypothesized that if the applied strain (stress) is instantaneously removed at point c then the sample will follow the path ca. The elastic energy recovered on this path is

$$e_{ca} = \frac{E_0\epsilon_0^2}{2}(1-\alpha). \tag{32}$$

Assume that the difference between the energy added and the energy recovered e_{ca} is lost in AE (aftershocks) and find that this energy e_{AE} which corresponds to the area of the triangle abc in Fig. 3(b) is given by

$$e_{AE} = e_{ab} - e_{ca} = \tfrac{1}{2}E_0\epsilon_0^2\alpha. \tag{33}$$

The rate of energy release is obtained by substituting Eq. (26) into (32) and taking the time derivative with the result

$$\frac{de_{AE}}{dt} = \frac{E_0\epsilon_0^4}{2t_d\epsilon_y^2}\left[\left(\frac{\epsilon_0}{\epsilon_y}-1\right)^{-(\rho-1)} + (\rho-1)\left(\frac{\epsilon_0}{\epsilon_y}\right)^3\left(\frac{t}{t_d}\right)\right]^{-\rho/(\rho-1)}. \tag{34}$$

The nondimensional rate of energy release $2t_d\epsilon_y^2/E_0\epsilon_0^4$ from Eq. (34) is given as a function of nondimensional time t/t_d in Fig. 5(b) taking $\rho = 2$ and several values of the applied nondimensional strain ϵ_0/ϵ_y. The transition to the power-law stress relaxation is clearly illustrated. The dependence of the nondimensional rate of energy release on nondimensional time is given in Fig. 5(d) taking $\epsilon_0/\epsilon_y = 2$ and several values of ρ. Again the power-law decay is clearly illustrated.

A universal scaling law is applicable to the temporal decay of aftershock activity following an earthquake. This is known as the modified Omori's law and as most widely used has the form [22]

$$\frac{dn_{as}}{dt} = \frac{C_1}{[C_2 + (t - t_{ms})]^p}, \tag{35}$$

where n_{as} is the number of aftershocks with magnitudes greater than a specified value, $t - t_{ms}$ is time measured forward from the occurrence of the mainshock at t_{ms}, C_1 and C_2 are constants, and the power p has a value somewhat greater than unity. Reasenberg and Jones [23] have carried out a detailed study of aftershocks for major earthquakes in California and find that $p = 1.07 \pm 0.03$.

Eq. (34) gives the rate of energy release whereas the modified Omori's law in Eq. (35) gives the rate of occurrence of aftershocks. However, it is recognized [23] that the frequency magnitude statistics are universal so that the rate of energy release is proportional to the rate of occurrence of earthquakes

$$\frac{de_{AE}}{dt} \propto \frac{dn_{as}}{dt}. \tag{36}$$

These two quantities have the same time dependence in Eqs. (34) and (35) if $p = \rho/(\rho-1)$. Taking $p = 1.07$ we find $\rho = 15.3$. This is a much higher value than that found for chipboard in Fig. 4, but the nucleation of rupture on preexisting faults would be expected to be a very different process than the nucleation in chipboard or fiberglass panels.

5. Stress increasing linearly with time

Next, consider the failure of a rod when the applied stress σ is increased linearly with time t.

This is a commonly applied condition when materials are stressed to failure in the laboratory. Assume that the stress on the sample is given by

$$\sigma(t) = \sigma_y \frac{t}{t_y}. \tag{37}$$

The rate of increase of applied stress $d\sigma/dt = \sigma_y/t_y$ is specified by giving the time t_y required to reach the yield stress σ_y. In the range of stresses $0 \leqslant \sigma \leqslant \sigma_y$ there is no damage and $\alpha = 0$; we assume elastic, reversible behavior of the material. Damage to the sample begins at $\sigma = \sigma_y$, that is when $t = t_y$. The equation for the rate of increase of damage in the range of stresses $\sigma_y < \sigma \leqslant \sigma_f$ is obtained from Eqs. (4), (6) and (37) with the result

$$\frac{d\alpha}{dt} = \frac{1}{t_d}\left(\frac{t}{t_y} - 1\right)^{\rho}\left[\frac{\epsilon(t)}{\epsilon_y}\right]^2. \tag{38}$$

From Eqs. (3) and (37) the strain $\epsilon(t)$ is related to the damage variable α and the applied stress σ by

$$\epsilon(t) = \epsilon_y\left(\frac{t}{t_y}\right)\frac{1}{1-\alpha(t)}. \tag{39}$$

Substitution of Eq. (39) into (38) gives the damage rate equation

$$\frac{d\alpha}{dt} = \frac{1}{t_d}\left(\frac{t}{t_y}\right)^2\left(\frac{t}{t_y} - 1\right)^{\rho}\frac{1}{[1-\alpha(t)]^2} \tag{40}$$

which can be integrated assuming an initial condition

$$\alpha = 0 \quad \text{when } t = t_y. \tag{41}$$

The solution of the first order differential equation (40) with the specified initial condition in Eq. (41) is given by

$$\alpha(t) = 1 - \left\{1 - 3\frac{t_y}{t_d}\left[\frac{1}{\rho+3}\left(\frac{t}{t_y} - 1\right)^{\rho+3} + \frac{2}{\rho+2}\left(\frac{t}{t_y} - 1\right)^{\rho+2} + \frac{1}{\rho+1}\left(\frac{t}{t_y} - 1\right)^{\rho+1}\right]\right\}^{1/3}. \tag{42}$$

The time evolution of the damage variable $\alpha(t)$ from Eq. (42) is shown in Fig. 6(a) for several values of the nondimensional loading rate t_y/t_d and $\rho = 2$. Failure occurs at $t = t_f$ when $\alpha = 1$. It is seen that a rapid loading rate, small t_y/t_d, leads to longer nondimensional failure times, large t_f/t_y. The dependence of the nondimensional failure time t_f/t_y on the loading rate t_y/t_d is obtained by setting $\alpha = 1$ in Eq. (42) with the result

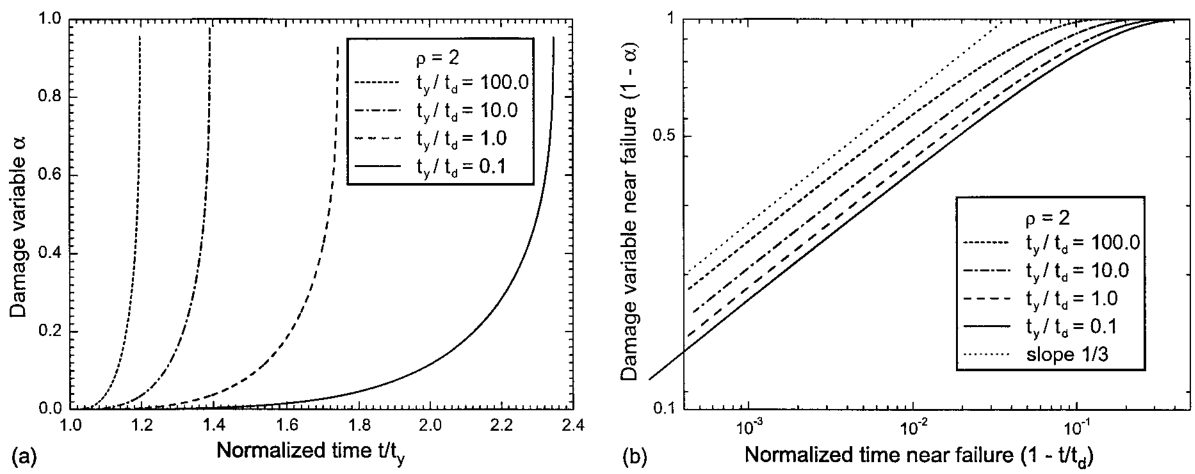

Fig. 6. (a) Dependence of the damage variable α on the nondimensional time t/t_d for several values of the nondimensional loading rate t_y/t_d. (b) Illustration of the power-law scaling of the damage variable α during the approach to failure when the applied stress is increased linearly with time.

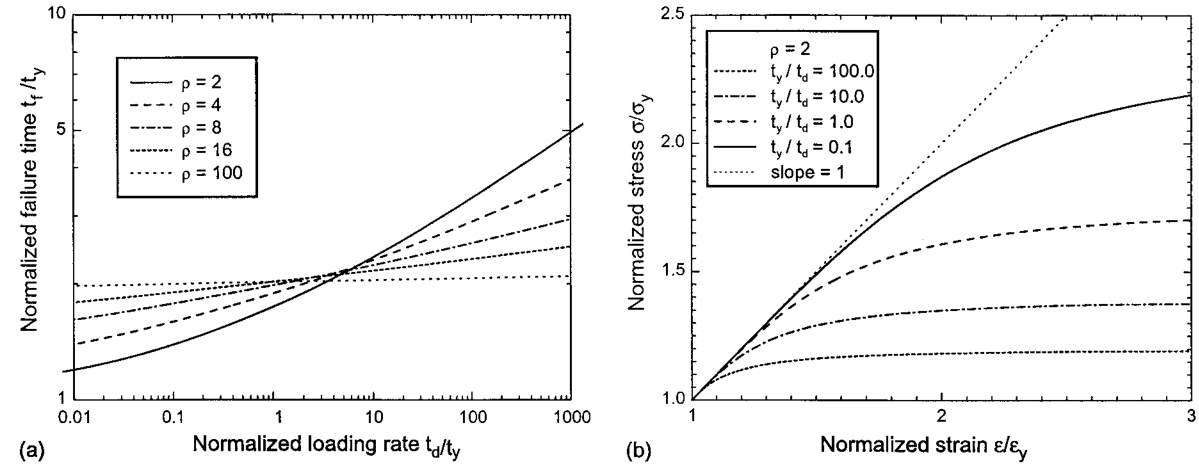

Fig. 7. (a) Dependence of the nondimensional failure time t_f/t_y on the nondimensional loading rate t_y/t_d when the applied stress is increased linearly with time. (b) Dependence of the nondimensional stress $\sigma(t)/\sigma_y$ on the nondimensional strain $\epsilon(t)/\epsilon_y$ during failure for several values of the nondimensional loading rate t_y/t_d.

$$\frac{t_d}{t_y} = 3\left[\frac{1}{\rho+3}\left(\frac{t_f}{t_y}-1\right)^{\rho+3} + \frac{2}{\rho+2}\left(\frac{t_f}{t_y}-1\right)^{\rho+2} + \frac{1}{\rho+1}\left(\frac{t_f}{t_y}-1\right)^{\rho+1}\right]. \tag{43}$$

This dependence is illustrated in Fig. 7(a). The nondimensional failure time t_f/t_y has a relatively weak dependence on the nondimensional loading rate t_y/t_d especially for higher values of ρ.

In order to study the approach to failure we plot $\log(1-\alpha)$ versus $\log(1-t/t_f)$ in Fig. 6(b). The straight line behavior indicates power-law scaling which is very close to the power 1/3 given for the application of a constant stress in Eq. (37). Thus, the power-law approach to failure is the same for constant stress and for a stress that increases linearly with time.

Section 3 showed that the experimental results in [9] on the failure of chipboard panels under rapid loading were in good agreement with the power-law scaling given in Eq. (13). The same experimental apparatus in [8] was used to study the failure of chipboard panels when the applied pressure difference P was increased linearly with time in accordance with Eq. (37). Their results are shown in Fig. 2(b). Again, after an initial transient, these authors found that the cumulative energy e_{AE} associated with AE events prior to rupture scaled as $e_{AE} \propto (1-t/t_f)^{-0.27}$. These authors found the same power-law time dependence for a linearly increasing pressure and for a suddenly applied constant pressure in agreement with our results using damage mechanics.

Next, consider the dependence of stress on strain during failure with an applied stress that is increasing linearly with time. The applicable stress–strain relation can be obtained from Eqs. (37), (39) and (42) with the result

$$\frac{\epsilon}{\epsilon_y} = \frac{\sigma}{\sigma_y}\left\{1 - 3\frac{t_y}{t_d}\left[\frac{1}{\rho+3}\left(\frac{\sigma}{\sigma_y}-1\right)^{\rho+3} + \frac{2}{\rho+2}\left(\frac{\sigma}{\sigma_y}-1\right)^{\rho+2} + \frac{1}{\rho+1}\left(\frac{\sigma}{\sigma_y}-1\right)^{\rho+1}\right]\right\}^{-1/3}. \tag{44}$$

This dependence is shown in Fig. 7(b) for several values of the nondimensional loading rate t_y/t_d. For very rapid loading, small t_y/t_d, the stress–strain curve approaches linear elasticity Eq. (1). For very slow loading, large t_y/t_d, the stress–strain curve approaches "equilibrium" failure with $\sigma = \sigma_y$. The results given in Fig. 7(b) show various failure paths through the metastable region defined in Fig. 1(b). The failure path BJ in Fig. 1(b) corresponds to the failure path with $t_y/t_d = 1$ in Fig. 7(b).

6. Strain increasing linearly with time

For the final example we will consider the behavior of a sample when the applied strain ϵ is increased linearly with time. This is another commonly applied condition in laboratory studies. In this case failure does not occur in our model and the stress on the sample first increases and then decreases as the strain and damage increases. Assume that the strain on the sample is given by

$$\epsilon(t) = \epsilon_y \frac{t}{t_y}. \tag{45}$$

The rate of increase of applied strain $d\epsilon/dt = \epsilon_y/t_y$ is specified by giving the time t_y required to reach the yield strain ϵ_y. In the range of strains $0 \leqslant \epsilon \leqslant \epsilon_y$ there is no damage and $\alpha = 0$. Damage to the sample begins at $\epsilon = \epsilon_y$, that is when $t = t_y$. The equation for the rate of increase of damage for strain $\epsilon > \epsilon_y$ is obtained from Eqs. (4), (6), and (45) with the result

$$\frac{d\alpha}{dt} = \frac{1}{t_d}\left[\frac{\sigma(t)}{\sigma_y} - 1\right]^{\rho}\left(\frac{t}{t_y}\right)^2. \tag{46}$$

From Eqs. (3) and (45) the stress $\sigma(t)$ is related to the damage variable $\alpha(t)$ and the applied strain $\epsilon(t)$ by

$$\sigma(t) = \sigma_y[1-\alpha(t)]\frac{\epsilon(t)}{\epsilon_y} = \sigma_y[1-\alpha(t)]\frac{t}{t_y}. \tag{47}$$

Using Eq. (47), it is possible to rewrite the damage rate equation (46) in the following form

$$\frac{d\alpha}{dt} = \frac{1}{t_d}\left\{[1-\alpha(t)]\frac{t}{t_y} - 1\right\}^{\rho}\left(\frac{t}{t_y}\right)^2. \tag{48}$$

The solution to Eq. (48) can be obtained only numerically. The damage starts to develop at time $t = t_y$ when the stress σ equals the yield stress σ_y. Therefore we use the initial condition $\alpha(t_y) = 0$. The time evolution of the damage variable $\alpha(t)$ from the numerical solutions of Eq. (48) is shown in Fig. 8(a) for several values of the nondimensional loading rate t_y/t_d and $\rho = 2$. In the damage model, failure does not occur since $\alpha \to 1$ only as $t \to \infty$. Our numerical solutions also give the dependence of stress on strain when the applied stress is increasing linearly with time. This dependence is shown in Fig. 8(b) for several values of the nondimensional loading rate t_y/t_d. It is seen that the stress first increases to a maximum value and then decreases with increasing strain (time). This stress relaxation is similar to that obtained in Section 4 with the instantaneous application of a

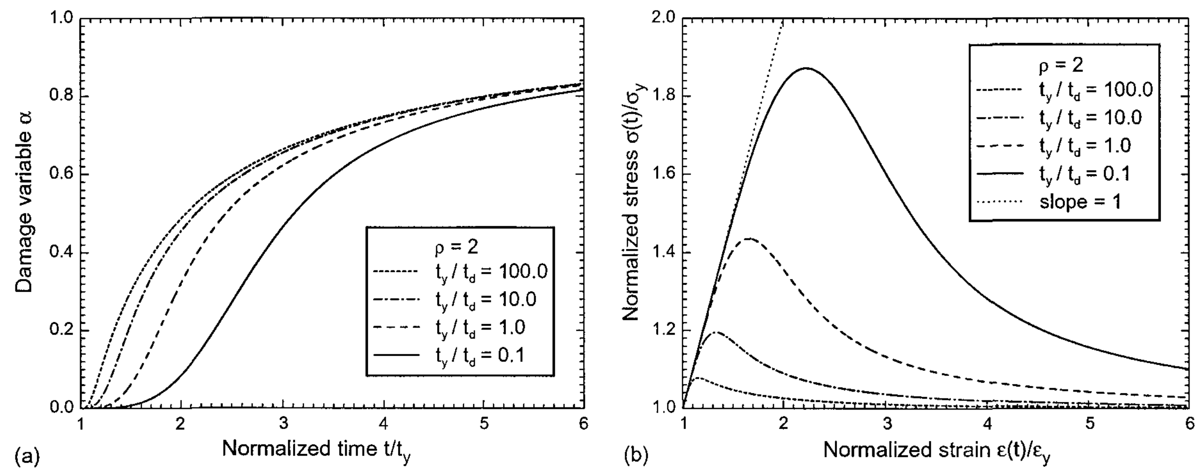

Fig. 8. (a) Dependence of the damage variable α on the nondimensional time t/t_y when the applied strain is increased linearly with time. (b) Dependence of the nondimensional stress $\sigma(t)/\sigma_y$ on the nondimensional strain $\epsilon(t)/\epsilon_y$.

constant strain. The maximum stress increases with increasing loading rate, small t_y/t_d.

7. Discussion

A widely used approach to the failure of a brittle material is damage mechanics. In this paper we have applied the generally accepted form of damage evolution to four relatively simple problems. The first is the instantaneous application of stress to a solid. If the applied stress exceeds the yield stress, damage increases until the solid fails at a well defined failure time. The results are applicable to the failure of chipboard panels. The problem of the damage of a solid subjected to an instantaneous strain was solved. If the applied strain exceeds the yield strain damage results in the relaxation of the stress to the yield stress. It is argued that this stress relaxation process is directly analogous to the temporal decay of the aftershock sequence following an earthquake. The rupture during an earthquake increases the strain and stress in some adjacent region. The aftershock sequence relaxes this added stress. In the last two examples we have also considered constant rates of addition of stress and strain.

Each type of solid requires its own formulation of constitutive equations which define the evolution of damage. A relevant measure as to the applicability of damage mechanics would be the amount of "disorder" in the solid. A pure crystalline material would have minimum disorder. Dislocations and microcracks would increase the disorder. Brittle composite materials have considerable built in disorder. It has been shown that there is a close association between damage mechanics and the failure of fiber-bundles [3,24]. Fiber-bundles are an accepted model for the failure of composite materials.

Damage mechanics is a quasi-empirical approach to the deformation of a brittle solid. However, the dependence of rate of damage generation on strain and stress in Eq. (4) has a thermodynamic basis [1,3,21]. The analogy we have made between phase changes and fracture also has a thermodynamic basis. Thermal fluctuations are crucial in phase changes of solids and liquids. A fundamental question is whether temperature plays a significant role in the damage of brittle materials.

Some forms of "damage" are clearly thermally activated. The deformation of solids by diffusion and dislocation creep is an example. The ability of vacancies and dislocations to move through a crystal is governed by an exponential dependence on absolute temperature with a well defined activation energy. The role of temperature in brittle fracture is unclear. The temperature in the experiments [8] for the fracture of chipboard and had no effect. A systematic temperature dependence of rate and state friction was documented by Nakatani [25]. This has also been shown to be true for the lifetime statistics of kevlar fibers [26].

Time delays associated with bubble nucleation in a superheated liquid are explained in terms of thermal fluctuations. The fluctuations must become large enough to overcome the stability associated with surface tension in a bubble. The fundamental question in damage mechanics is the cause of the delay in the occurrence of damage. This problem has been considered in some detail in [27]. These authors attributed damage to the "thermal" activation of microcracks. An effective "temperature" can be defined in terms of the spatial disorder (heterogeneity) of the solid. The spatial variability of stress in the solid is caused by the microcracking itself, not by thermal fluctuations. This microcracking occurs on a wide range of scales.

Acknowledgements

The authors would like to thank Yehuda Ben-Zion, Bill Klein, William Newman, Leigh Phoenix, John Rundle, and Charlie Sammis for many valuable and stimulating discussions.

References

[1] L.M. Kachanov, Introduction to Continuum Damage Mechanics, Martinus Nijhoff, Dordrecht, Netherlands, 1986.
[2] J. Lemaitre, J.-L. Chaboche, Mechanics of Solid Materials, Cambridge University Press, Cambridge, 1990.

[3] D. Krajcinovic, Damage Mechanics, Elsevier, Amsterdam, 1996.
[4] L.B. Freund, Dynamic Fracture Mechanics, Cambridge University Press, Cambridge, 1990.
[5] K. Mogi, Study of elastic shocks caused by the fracture of heterogeneous materials and its relations to earthquake phenomena, Bull. Earthquake Res. Insti. 40 (1962) 125–173.
[6] H. Otani, S.L. Phoenix, P. Petrina, Matrix effects on lifetime statistics for carbon fibre–epoxy microcomposites in creep rupture, J. Mat. Sci. 26 (1991) 1955–1970.
[7] A. Johansen, D. Sornette, Critical ruptures, Eur. Phys. J. B18 (2000) 163–181.
[8] A. Guarino, A. Garcimartin, S. Ciliberto, An experimental test of the critical behavior of fracture precursors, Eur. Phys. J. B6 (1998) 13–24.
[9] A. Guarino, S. Ciliberto, A. Garcimartin, Failure time and microcrack nucleation, Europhys. Lett. 47 (1999) 456.
[10] A. Buchel, J.P. Sethna, Statistical mechanics of cracks: Fluctuations, breakdown, and asymptotics of elastic theory, Phys. Rev. E 55 (1997) 7669–7690.
[11] S. Zapperi, P. Ray, H.E. Stanley, A. Vespignani, First-order transition in the breakdown of disordered media, Phys. Rev. Lett. 78 (1997) 1408–1411.
[12] F. Kun, H.J. Herrmann, Transition from damage to fragmentation in collision of solids, Phys. Rev. E 59 (1999) 2623–2632.
[13] D. Sornette, J.V. Andersen, Scaling with respect to disorder in time-to-failure, Eur. Phys. J. B 1 (1998) 353–357.
[14] S. Gluzman, D. Sornette, Self-consistent theory of rupture by progressive diffuse damage, Phys. Rev. E 63 (2001) 066129.
[15] R.L.B. Selinger, Z.G. Wang, W.M. Gelbart, A. Ben-Shaul, Statistical-thermodynamic approach to fracture, Phys. Rev. A 43 (1991) 4396–4400.
[16] J.B. Rundle, W. Klein, S. Gross, Dynamics of a traveling density wave model for earthquakes, Phys. Rev. Lett. 76 (1996) 4285–4288.
[17] J.B. Rundle, W. Klein, S. Gross, Physical basis for statistical patterns in complex earthquake populations: models, predictions and tests, Pure Appl. Geophys. 155 (1999) 575–607.
[18] J.B. Rundle, W. Klein, D.L. Turcotte, B.D. Malamud, Precursory seismic activation and critical point phenomena, Pure Appl. Geophys. 157 (2000) 2165–2182.
[19] S. Zapperi, P. Ray, H.E. Stanley, A. Vespignani, Avalanches in breakdown and fracture processes, Phys. Rev. E 59 (1999) 5049–5057.
[20] P.G. Debenedetti, Metastable Liquids, Princeton University Press, Princeton, 1996.
[21] V. Lyakhovsky, Y. Ben-Zion, A. Agnon, Distributed damage, faulting and friction, J. Geophys. Res. 102 (1997) 27, 635–727.
[22] C.H. Scholz, The Mechanics of Earthquakes and Faulting, Cambridge University Press, Cambridge, 2002.
[23] P.A. Reasenberg, L.M. Jones, Science 243 (1989) 1173–1176.
[24] D.L. Turcotte, W.I. Newman, R. Shcherbakov, Micro- and macro-scopic models of rock fracture, Geophys. J. Int., 2003, in press.
[25] M. Nakatani, Conceptual and physical clarification of rate and state friction: Frictional sliding as a thermally activated rheology, J. Geophys. Res. 106 (2001) 13, 347–413.
[26] H.F. Wu, S.L. Phoenix, P. Schwartz, Temperature dependence of lifetime statistics for single Kevlar 49 filaments in creep-rupture, J. Mat. Sci. 23 (1998) 1851–1860.
[27] S. Ciliberto, A. Guarino, R. Scorretti, The effect of disorder on the fracture nucleation process, Physica D 158 (2001) 83–104.